Journal of Alloys and Compounds 587 (2014) 755–762

Contents lists available at ScienceDirect

Journal of Alloys and Compounds

journal homepage: www.elsevier.com/locate/jalcom

Hydrothermal synthesis of Gd_2O_3:Eu^{3+} nanophosphors: Effect of surfactant on structural and luminescence properties

N. Dhananjaya [a,b,*], H. Nagabhushana [c,*], S.C. Sharma [a,d], B. Rudraswamy [e], C. Shivakumara [f], B.M. Nagabhushana [g]

[a] B.S. Narayan Centre of Excellence for Advanced Materials, B.M.S. Institute of Technology, Bangalore 560 064, India
[b] Department of Physics, B.M.S. Institute of Technology, Bangalore 560 064, India
[c] Prof. C.N.R. Rao Centre for Advanced Materials, Tumkur University, Tumkur 572 103, India
[d] Department of Mechanical Engineering, B.M.S. Institute of Technology, Bangalore 560 064, India
[e] Department of Physics, J.B. Campus, Bangalore University, Bangalore 560 056, India
[f] Solid State and Structural Chemistry Unit, Indian Institute of Science, Bangalore 560 012, India
[g] Department of Chemistry, M.S. Ramaiah Institute of Technology, Bangalore 560 054, India

ARTICLE INFO

Article history:
Received 9 August 2013
Received in revised form 14 October 2013
Accepted 15 October 2013
Available online 26 October 2013

Keywords:
Nanophosphor
Gadolinium oxide
Photoluminescence
HDA

ABSTRACT

Various morphologies of Eu^{3+} activated gadolinium oxide have been prepared by hydrothermal method using hexadecylamine (HDA) as surfactant at different experimental conditions. The powder X-ray diffraction studies reveal as-formed product is hexagonal $Gd(OH)_3$:Eu^{3+} phase and subsequent heat treatment at 350 and 600 °C transforms to monoclinic GdOOH:Eu^{3+} and cubic Gd_2O_3:Eu^{3+} phases respectively. SEM pictures of without surfactant show irregular shaped rods along with flakes. However, in the presence of HDA surfactant, the particles are converted into rods of various sizes. The temperature dependent morphological evolution of Gd_2O_3:Eu^{3+} without and with HDA surfactant is studied. TEM micrographs of $Gd(OH)_3$:Eu^{3+} sample with HDA confirms smooth nanorods with various diameters in the range 20–100 nm. FTIR studies reveal that HDA surfactant plays an important role in conversion of cubic to hexagonal phases. Among these three phases, cubic phase Gd_2O_3:Eu^{3+} (λ_{ex} = 254 nm) show red emission at 612 nm corresponding to $^5D_0 \rightarrow {}^7F_2$ and is more efficient host than the monoclinic counterpart. The band gap for hexagonal $Gd(OH)_3$:Eu^{3+} is more when compared to monoclinic GdOOH:Eu^{3+} and cubic Gd_2O_3:Eu^{3+}.

© 2013 Elsevier B.V. All rights reserved.

1. Introduction

Rare earth compounds are an important family of inorganic material that have been widely used as luminescent devices, catalysts, magnetic materials, flourescent labels for biological detection and other functional materials based on the electronic, optical and chemical characteristics resulting from their unique 4f electron configuration [1–5]. Gd_2O_3 show good luminescent properties when doped with rare earth ions (Eu^{3+}) and it is an ideal system for fundamental research such as energy transfer from Gd^{3+} to Eu^{3+}. Especially cubic Gd_2O_3:Eu^{3+} has widely used as X-ray scintillator materials plasma display panel (PDP), flat panel displays, projection televisions etc. Gd_2O_3 is a versatile material with high application potential in several technological fields (photonics) due to its transparency from visible to near-infrared region.

Gd_2O_3:Eu^{3+} exhibits strong paramagnetic behavior (S = 7/2) as well as strong UV and cathode ray excited luminescence, up conversion behavior when it is doped with Sm^{3+}, Er^{3+} and also as an efficient Thermoluminescence (TL) phosphor. Various chemical methods are used for the preparation of rare earth oxides including combustion [6], solvothermal [7], wet chemical approach [8], microwave [9] etc. sometimes the final product obtained from these methods show mixed phases and cannot achieved direct phase. In recent years, hydrothermal method is widely used to prepare the nanostructure materials because of its simplicity, high efficiency [10,11]. The synthesis of these nanostructures is based on the subsequent hydrothermal treatment at a designated temperature. To the best of our knowledge, various phases of gadolinium oxide using HDA surfactant are very limited. In the present study, we have investigated effect HDA surfactant on luminescence properties of Eu^{3+} doped $Gd(OH)_3$, GdOOH and Gd_2O_3.

* Corresponding authors. Address: B.S. Narayan Centre of excellence for Advanced Materials, B.M.S. Institute of Technology, Bangalore 560 064, India (N. Dhananjaya). Tel.: +91 9036840280.
E-mail addresses: dhanu.siri@yahoo.co.in (N. Dhananjaya), bhushanvlc@gmail.com (H. Nagabhushana).

0925-8388/$ - see front matter © 2013 Elsevier B.V. All rights reserved.
http://dx.doi.org/10.1016/j.jallcom.2013.10.121

2. Experimental

2.2. Synthesis of Eu^{3+} doped $Gd(OH)_3$, GdOOH and Gd_2O_3 nanorods with and without HDA surfactant

The $Gd(OH)_3:Eu^{3+}$ (4 mol%) is synthesized by hydrothermal method at 120 °C for 24 h, maintained ~12 pH. All the chemical reagents used in the present experiments are obtained from commercial sources. In a typical synthesis, the stoichiometric amounts of Gd_2O_3 and Eu_2O_3 [2.51 g (6.9 m mol) of Gd_2O_3 and 0.10 g (0.29 m mol) of Eu_2O_3] are dissolved in 1:1 HNO_3. A clear solution is obtained after uniform stirring and thereafter the solution is heated on the sand bath to evaporate excess HNO_3. The aqueous KOH (1.0 N) solution is added into the mixture until the pH of solution is adjusted to ~12. The addition of KOH solution to adjust the pH to be higher than 11 significantly reduces the aspect ratio of $Gd(OH)_3:Eu^{3+}$ particles to produce essentially nanorods [12]. It is suggested that the high OH^- ion concentration is preferably for one-dimensional growth [13]. This would imply that an optimal pH condition is required for the growth of true nanorods with high aspect ratio. The resulting colloidal mixture is put into a Teflon-lined stainless steel autoclave with a capacity of 60 mL. The autoclave is then sealed and maintained at 120 °C for 24 h and thereafter naturally cooled to room temperature. A white solid product of $Gd(OH)_3:Eu^{3+}$ is collected by filtration and washed several times with distilled water and ethyl alcohol and then dried at 80 °C. Subsequent dehydration of $Gd(OH)_3:Eu^{3+}$ by heat treatment at 350 and 600 °C for 3 h results in monoclinic $GdOOH:Eu^{3+}$ and cubic $Gd_2O_3:Eu^{3+}$, respectively. Further, the effect of HDA (0.0241 g; 1 mol%) surfactant on each phase is studied by maintaining similar synthesis conditions (120 °C for 24 h) as well as heat treatments. HDA is a cationic surfactant and it plays a key role in controlling the growth and production of Gd_2O_3 nanorods. The growth process of Gd_2O_3 in the presence of HDA is different when the surface tension of solution is reduced to the existence of surfactant, which lowers the energy needed for the formation of a new phase. HDA is anionic compound, which ionizes completely in water. Fig. 1 shows the flow chart for the synthesis of different phases of Eu^{3+} activated $Gd(OH)_3$, GdOOH and Gd_2O_3 nanorods by the hydrothermal method with and without HDA surfactant.

2.3. Instruments used

The phase purity of the nanophosphors is examined by powder X-ray diffractometer (PXRD) (PANalytical XPert Pro) using Cu Kα radiation (λ = 1.5405A) with a nickel filter to estimate the crystallinity of the phases. The surface morphology of the samples have been examined using Scanning electron microscopy (JEOL JSM 840A) by sputtering technique with gold as covering contrast material. Transmission Electron Microscopy (TEM) analysis is performed on a Hitachi H-8100 (accelerating voltage up to 200 kV, LaB_6 filament) equipped with EDS (Kevex Sigma TM Quasar, USA). The UV–Vis spectra have been recorded on a UV-3101 Shimadzu spectrometer. The photoluminescence studies have been carried out using a Perkin–Elmer LS-55 luminescence spectrophotometer equipped with Xe lamp (excitation wavelength 250 nm). Raman spectroscopic studies have been performed using a Renishaw In-via Raman spectrometer equipped with a CCD (charge coupled device) with 633 nm (He–Cd laser power set at 30 mW) and a Leica DMLM optical microscope.

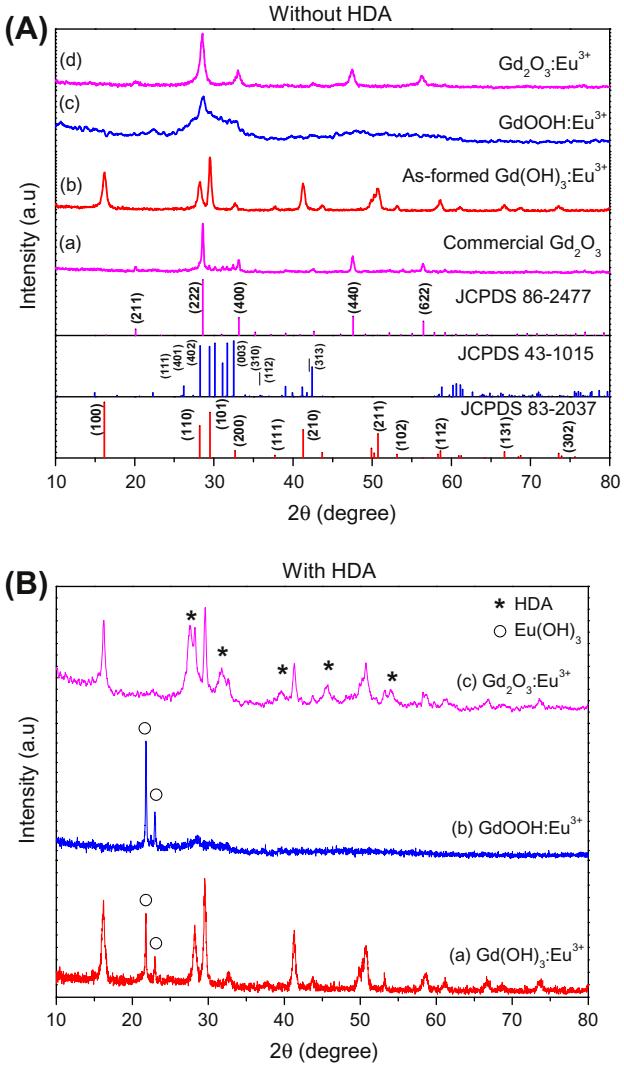

Fig. 2. (A) PXRD patterns of $Gd(OH)_3:Eu^{3+}$ prepared by without HDA (a) commercial Gd_2O_3, (b) as-formed, (c) calcined at 350 °C and (d) calcined at 600 °C and (B) With HDA (a) as-formed, (b) calcined at 350 °C and (c) calcined at 600 °C for 3 h.

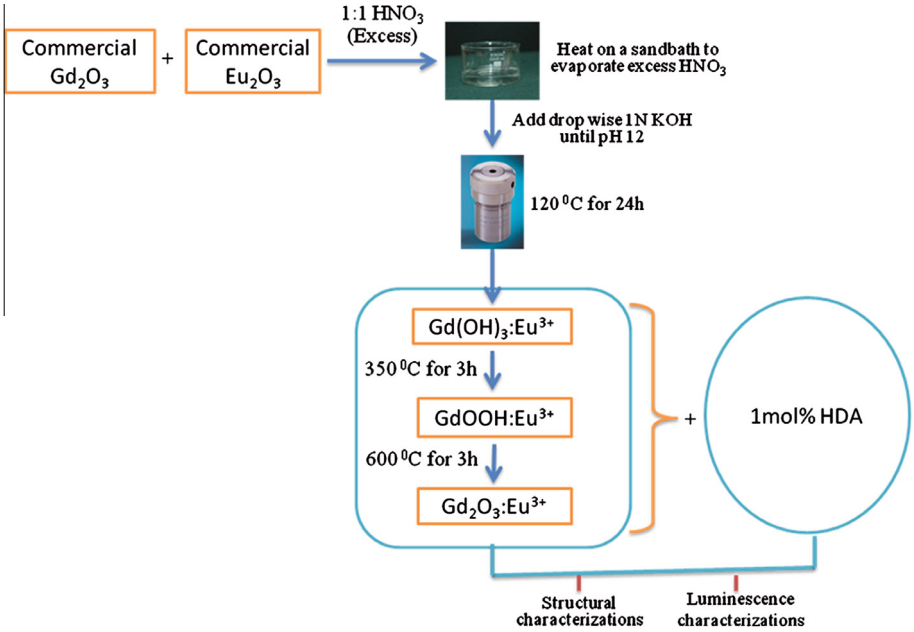

Fig. 1. Flow chart for the synthesis of $Gd_2O_3:Eu^{3+}$(HDA).

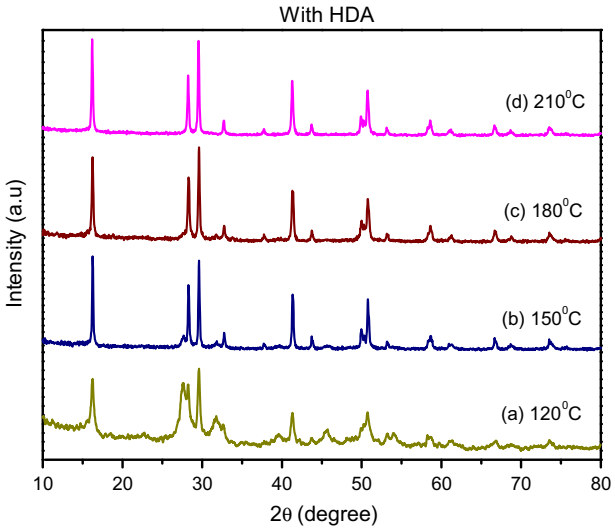

Fig. 3. PXRD patterns of cubic Gd_2O_3:Eu^{3+} (with HDA) at (a) 120 °C, (b)1 50 °C, (c)180 °C and (d) 210 °C for 24 h.

3. Results and discussion

The PXRD patterns of commercial Gd_2O_3 (Fig. 2A(a)) along with different phases of Eu^{3+} activated gadolinium ($Gd(OH)_3$; GdOOH and Gd_2O_3) without HDA surfactant is shown in (Fig. 2A(b–d)) respectively. The as-formed product shows hexagonal $Gd(OH)_3$:-Eu^{3+} which is consistent with the standard JCPDS file No. 83–2037. Upon heat treatment at 350 °C, PXRD patterns shows mixed phase of monoclinic GdOOH (JCPDS file 43-1015) and further heat treatment at 600 °C show, pure cubic phase Gd_2O_3:-Eu^{3+} (JCPDS file 86-2477).

Fig. 2B (a–c) shows the PXRD patterns of $Gd(OH)_3$:Eu^{3+}, GdOOH:Eu^{3+}, Gd_2O_3:Eu^{3+} in the presence of HDA surfactant respectively. The PXRD patterns of as formed samples show some additional impurity peaks of $Eu(OH)_3$ around 21.7° and 22.9° in Gd(OH):Eu^{3+} and GdOOH:Eu^{3+} phases and 27.5°, 31.6°, 39.55°, 45.63° in Gd_2O_3:Eu^{3+} phase which are due to HDA surfactant. The PXRD patterns of cubic Gd_2O_3:Eu^{3+} with HDA at different synthesis temperatures (120–210 °C) is studied as shown in Fig. 3. It is observed that the HDA impurities still remains at 120 °C for 24 h. However, with increase of synthesis temperature 150 °C and

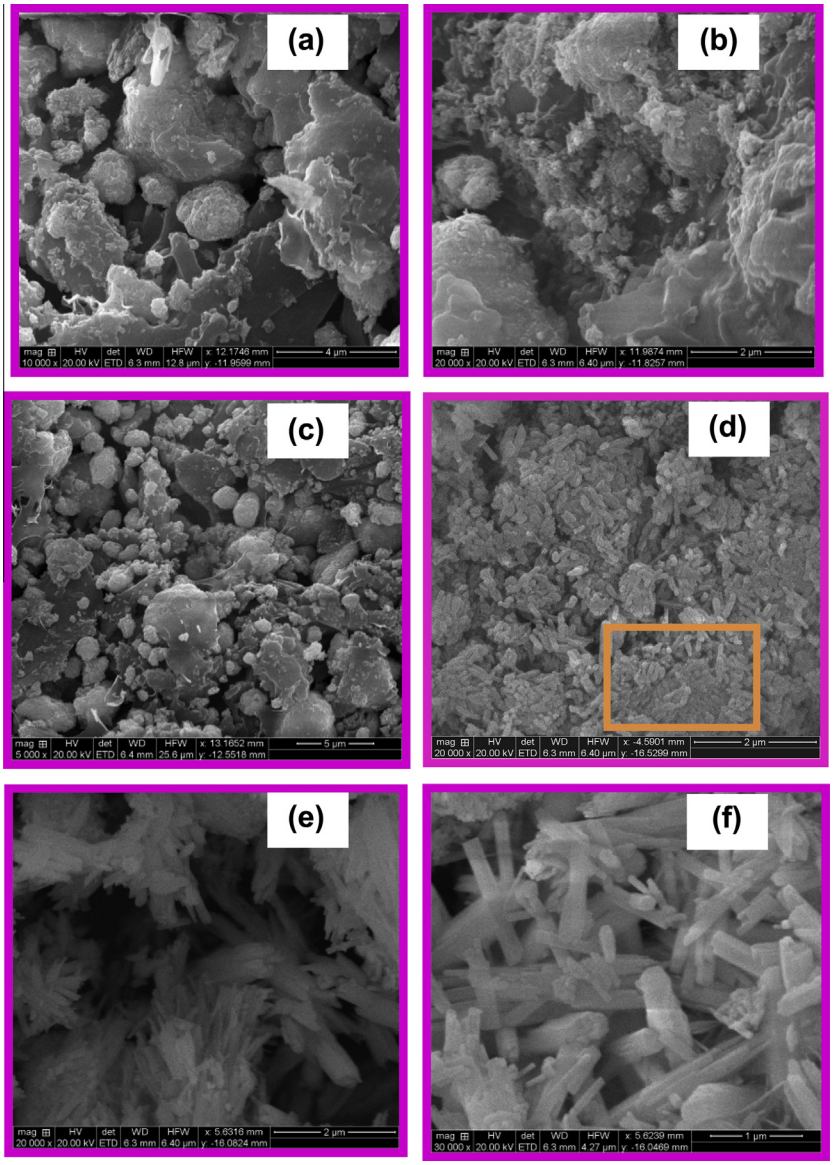

Fig. 4. SEM micrographs of (a) $Gd(OH)_3$:Eu^{3+}, (b) GdOOH:Eu^{3+} and (c) Gd_2O_3:Eu^{3+} prepared without HDA and (d) $Gd(OH)_3$: Eu^{3+}, (e) GdOOH: Eu^{3+} and (f) Gd_2O_3: Eu^{3+} prepared with HDA for 24 h.

180 °C, HDA impurity peaks are completely disappear. With further increase in synthesis temperature to 210 °C a pure hexagonal phase is obtained (Fig. 3d).

Fig. 4(a–c) shows SEM micrographs of $Gd(OH)_3:Eu^{3+}$, $GdOOH:Eu^{3+}$ and $Gd_2O_3:Eu^{3+}$ phases respectively, maintained at 120 °C for 24 h. It can be seen from the micrographs that the particles are fused and agglomerated in as-formed samples. However, when HDA is added to the respective phases (Fig. 4(d–f)) agglomeration is almost retained in $Gd(OH)_3:Eu^{3+}$ phase and for other two phases, agglomeration is reduced with more irregular shaped tapered end nanorods are observed. The temperature dependent (120–210 °C for 24 h) morphological evolution of $Gd_2O_3:Eu^{3+}$ with HDA is investigated by SEM and the images are shown in Fig. 5(a–d). The nanorods of irregular shape, branching with sharp tips, have been observed. As the temperature is raised to 180 °C for 24 h (Fig. 5a–c), nanorods of smooth and uniform diameter with varying lengths from 100 to 150 nm have been obtained. In this condition sharp edges are almost completely decomposed. At 210 °C for 24 h (Fig. 5d), the nanorods obtained are non-uniform and irregular in shape. In the present investigation, hydrothermal temperature of 180 °C for 24 h (Fig. 5c) is more suitable to obtain the smooth uniform nanorods.

Fig. 6 shows the typical TEM image of the $Gd(OH)_3:Eu^{3+}$ phosphors with HDA. The $Gd(OH)_3:Eu^{3+}$ nanorods exhibit relatively straight, smooth surface and the diameter varies in the range of 20–100 nm with different lengths. FTIR spectra of $Gd(OH)_3:Eu^{3+}$ without HDA is shown in Fig. 7A. The absorption peaks of H_2O at 3410 cm^{-1} and OH groups are observed at 703 and 3616 cm^{-1} [14]. The CO_3^{2-} anion groups are observed at ~1374 and ~1586 cm^{-1}, which indicate that the precursor might be hydroxyl carbonate. In $GdOOH:Eu^{3+}$ (Fig. 7A(c)) phase, the absorption peaks of H_2O at 3410 cm^{-1} and the CO_3^{2-} anion groups at 1498, 1383, 847 and 694 cm^{-1} have been observed. The strong absorption peak near 540 cm^{-1}, which is associated with the vibration of the Gd–O bond and the absorption peaks of H_2O at 3410 cm^{-1}. The CO_3^{2-} anion group is observed at 1489 cm^{-1}. Fig. 7B(a) and (b) show the FTIR spectra of $Gd(OH)_3:Eu^{3+}$ and $GdOOH:Eu^{3+}$ with HDA, respectively. It is noted that there is no change in the $Gd(OH)_3:Eu^{3+}$ and $GdOOH:Eu^{3+}$ phases after HDA, surfactant is added. Further, it is observed that HDA surfactant plays an important role in converting cubic $Gd_2O_3:Eu^{3+}$ to hexagonal $Gd(OH)_3:Eu^{3+}$ (Fig. 7B(c)).

Raman spectroscopy is a very powerful tool for characterizing nanomaterials because it is in situ and nondestructive method. Raman spectra of hexagonal $Gd(OH)_3:Eu^{3+}$, monoclinic $GdOOH:Eu^{3+}$ and cubic $Gd_2O_3:Eu^{3+}$ along with commercial Gd_2O_3 has been shown in Fig. 8(a-d). According to factor group analysis [15], there are 21 Raman bands in monoclinic phase, 10 active Raman bands for hexagonal and 22 Raman active bands in cubic phase [16] is predicted. The wavenumbers and the corresponding assignments are reported in Table 1. These Raman bands have been well comparable to those studied by different authors [17–19]. However, we have observed ~306, 385 and 488 cm^{-1} clear bands for hexagonal phase. Around 900 cm^{-1} for monoclinic phase and ~300, 361, 415, 441 and 481 cm^{-1} for cubic phase. The difference between the number of observed and predicted wavenumbers for these phases have been attributed to some weaker features which are not well defined in the Raman spectrum.

Fig. 9A and B show the UV–Vis absorbance spectra of without and with HDA hexagonal $Gd(OH)_3:Eu^{3+}$, monoclinic $GdOOH:Eu^{3+}$ and cubic $Gd_2O_3:Eu^{3+}$ respectively. A prominent absorption peak at 245 nm is observed in all the phases. The weak absorption peak in hexagonal $Gd(OH)_3:Eu^{3+}$ is shifted from 284 to 292 nm. The maximum absorption, which can be due to transition between valence band to conduction band [20]. The weak absorption in the UV–visible region is expected to arise from transitions involving extrinsic states such as surface traps or defect states or impurities [21].

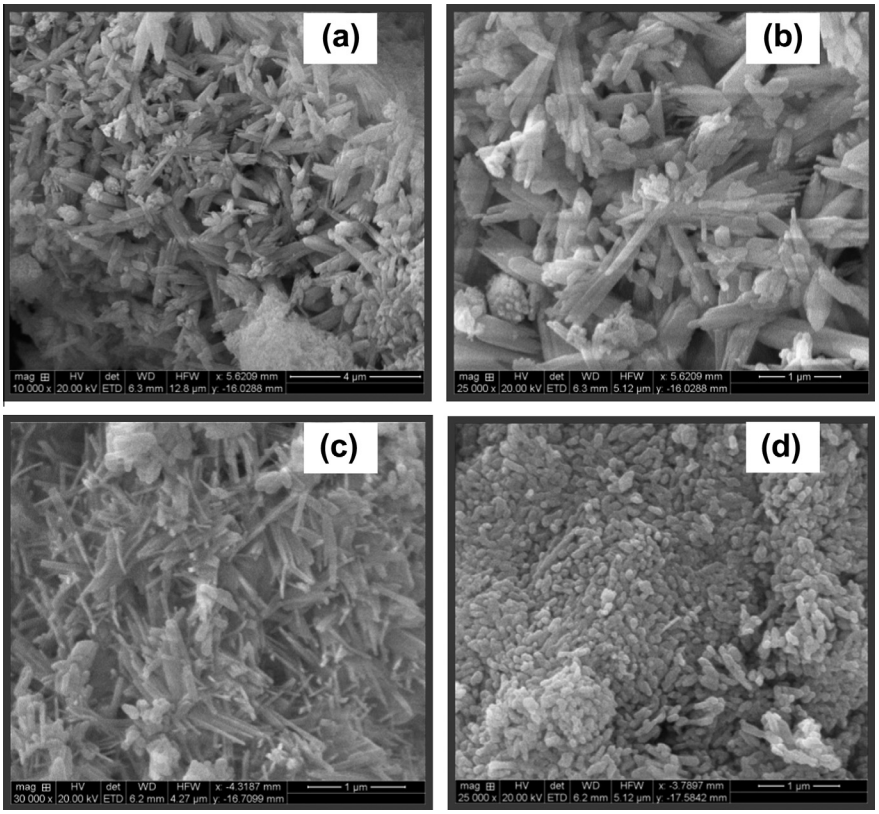

Fig. 5. SEM micrographs of cubic $Gd_2O_3:Eu^{3+}$ (with HDA) at (a) 120 °C, (b) 150 °C, (c) 180 °C and (d) 210 °C for 24 h.

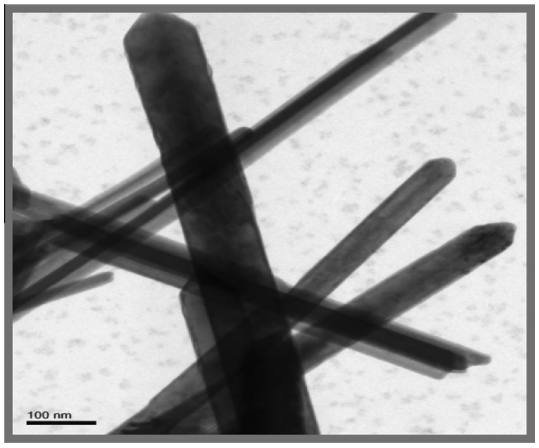

Fig. 6. TEM image of $Gd(OH)_3:Eu^{3+}$ nanorods.

The optical band gap energy (E_g) (Fig. 10A and B) has been estimated by the method proposed by Wood and Tauc [22]. The optical band gap is associated with absorbance and photon energy by the following equation:

$$E \propto A(h\upsilon - E_g)^k \quad (1)$$

where A – absorbance, h – Planck constant, υ – frequency, E_g – optical band gap and k is a constant associated to the different types of electronic transitions (k = 1/2, 2, 3/2 or 3 for direct allowed, indirect allowed, direct forbidden and indirect forbidden transitions, respectively). According to the literature [23], the oxides are characterized by an indirect allowed electronic transition and hence, the k = 2 value is used as standard in Eq. (1). Thus, the E_g values have been evaluated by extrapolating the linear portion of the curve or tail $[(h\upsilon\alpha)^{1/k} = 0]$ in the UV–Vis absorbance spectra. The optical energy band gap for commercial Gd_2O_3, hexagonal $Gd(OH)_3$: Eu^{3+}, monoclinic $GdOOH:Eu^{3+}$ and cubic $Gd_2O_3:Eu^{3+}$ without HDA is found to be 5.38, 5.68, 5.55, and 5.46 eV respectively and with HDA it is found to be 5.93, 4.83 and 5.41 for hexagonal $Gd(OH)_3:Eu^{3+}$, monoclinic $GdOOH:Eu^{3+}$ and cubic $Gd_2O_3:Eu^{3+}$ respectively. These values are well matched to those reported in literature [24]. It is observed that E_g value corresponding to $Gd(OH)_3:Eu^{3+}$ phase is more when compared to other two phases. This variation in energy gap might be attributed to different Gd_2O_3 oxide phases. Further, these variations in E_g can be related to the degree of structural order–disorder into the lattice, which is able to change the intermediary energy level distribution within the band gap.

The excitation spectra of without and with HDA surfactant of $Gd_2O_3:Eu^{3+}$ is shown in Fig. 11. The peak near 254 nm in the excitation spectra of $Gd_2O_3:Eu^{3+}$ without HDA is known as the charge transfer (CT) peak which attributes to the transition from O^{2-} 2p state to Eu^{3+} 4f state [25]. The broad peak at 235 nm originates from the excitation of Gd_2O_3 host lattice (HL). However, with HDA $Gd_2O_3:Eu^{3+}$, a single broad peak at 240 nm is observed. It is observed that HL peak in with HDA surfactant is shifted to ~5 nm when compared to without HDA samples. However, the CT peak is completely disappears with HDA surfactant. The HL and CT peaks of the with HDA samples are improved distinctly in comparison with that of without HDA samples.

Fig. 12 A and B shows the PL emission spectra of without and with HDA of $Gd(OH)_3:Eu^{3+}$, $GdOOH:Eu^{3+}$ and $Gd_2O_3:Eu^{3+}$ phases under 254 nm excited wavelength respectively. The Photoluminescence spectra of $Gd_2O_3:Eu^{3+}$ with HDA at different temperature are shown in Fig. 13. A weak and broad emission peaks in the range 600–650 in $Gd(OH)_3:Eu^{3+}$ and monoclinic $GdOOH:Eu^{3+}$ phases. However in the case of cubic $Gd_2O_3:Eu^{3+}$ a series of well developed

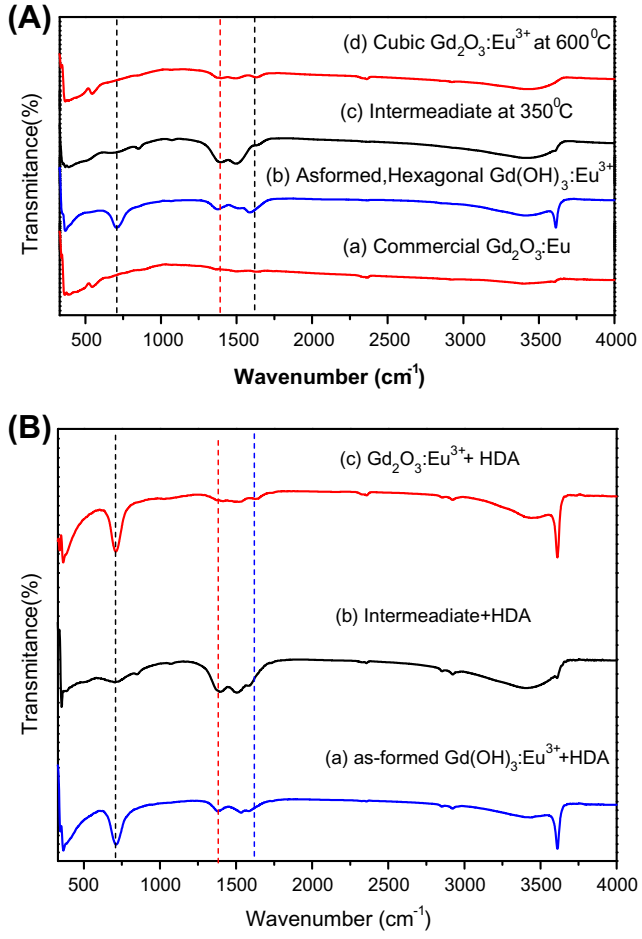

Fig. 7. (A) FTIR spectra of $Gd(OH)_3:Eu^{3+}$ prepared by without HDA (a) commercial Gd_2O_3, (b) as-prepared, (c) calcined at 350 °C and (d) calcined at 600 °C and (B) with HDA (a) as-prepared, (b) calcined at 350 °C and (c) calcined at 600 °C for 3 h.

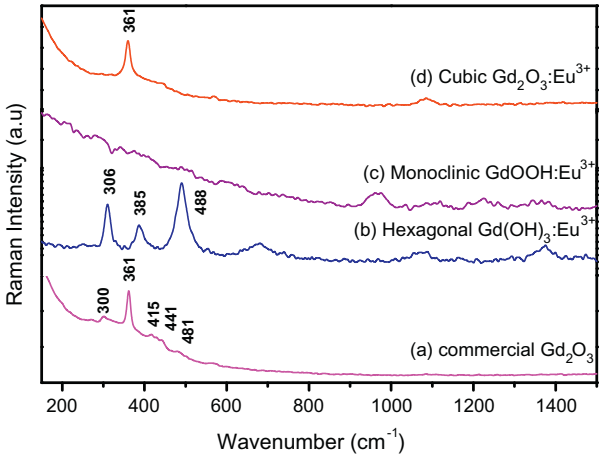

Fig. 8. Raman spectra of (without HDA) (a) commercial Gd_2O_3 and $Gd(OH)_3:Eu^{3+}$ prepared at (b) as-formed. (b) Calcined at 350 °C (b) calcined at 600 °C for 3 h.

Table 1
Raman assignments for hexagonal $Gd(OH)_3:Eu^{3+}$ and cubic $Gd_2O_3:Eu^{3+}$.

Phase	Wavenumbers (cm^{-1})	Assignment
Hexagonal	306, 385, 488	A_g
Cubic	300, 361, 415, 441, 481	$F_g + E_g$

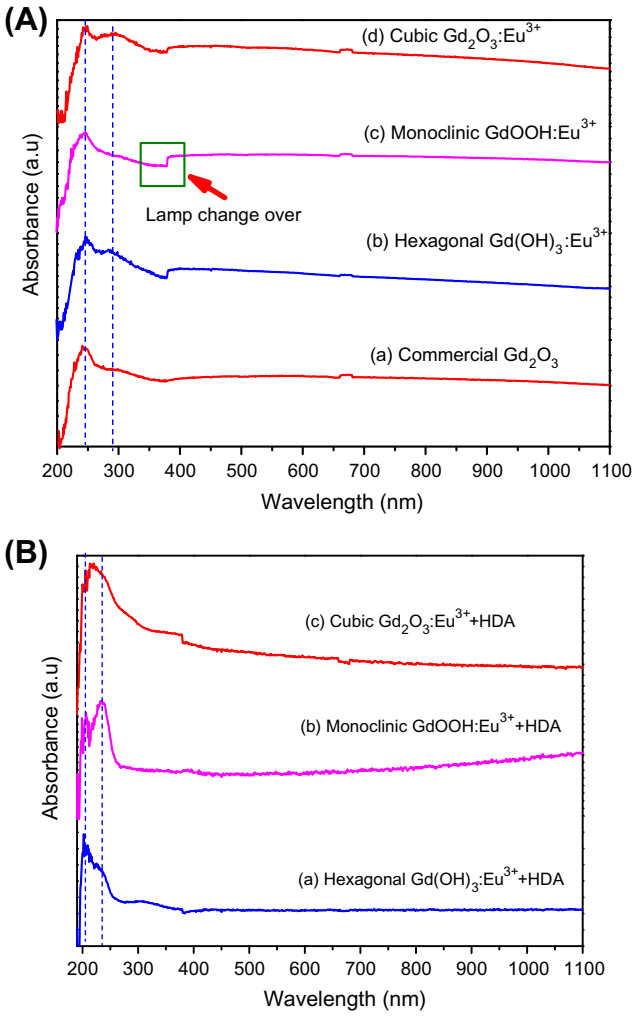

Fig. 9. (A) UV–Vis spectra of $Gd(OH)_3$:Eu^{3+} prepared (without HDA) (a) Commercial Gd_2O_3, (b) as-prepared, (c) calcined at 350 °C and (d) calcined at 600 °C for 3 h. And (B) with HDA (a) as-prepared, (b) calcined at 350 °C and (c) calcined at 600 °C for 3 h.

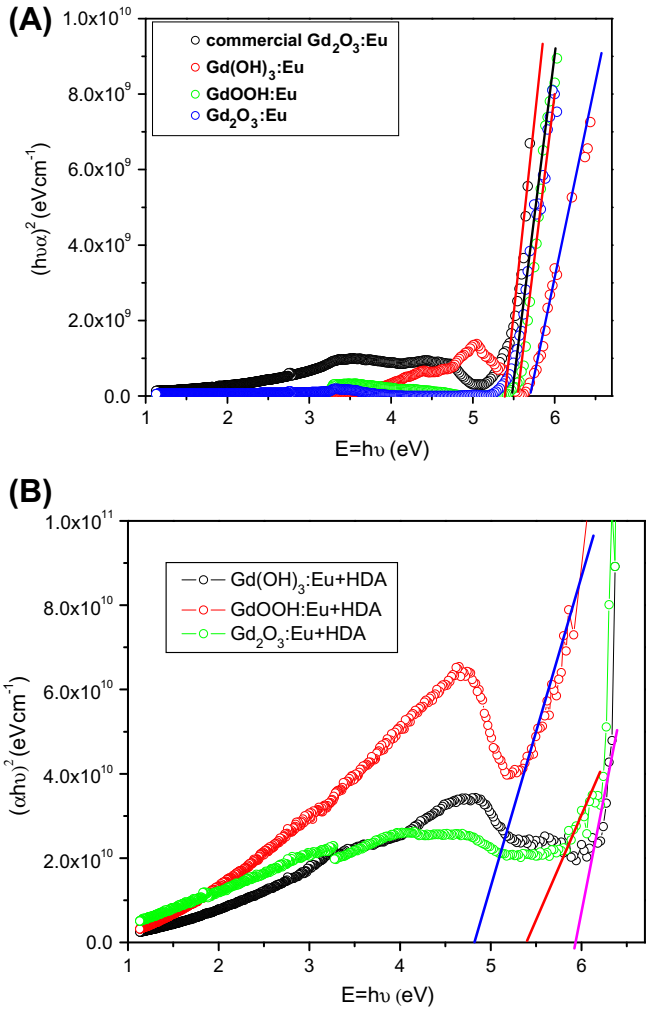

Fig. 10. (A) Energy gap of $Gd(OH)_3$:Eu^{3+} prepared (without HDA) (a) Commercial Gd_2O_3, (b) as-prepared, (c) calcined at 350 °C and (d) calcined at 600 °C for 3 h. (B) With HDA (a) as-prepared, (b) calcined at 350 °C and (c) calcined at 600 °C for 3 h.

emission peaks at 485, 533, 595, 611, 623, 649 nm are observed. Further same excitation wavelength is used for with HDA (1 mol%) samples. It shows similar emission peaks. The emission peaks for $^5D_0 \rightarrow {}^7F_2$ transition is consistent with the hexagonal $Gd(OH)_3$:Eu^{3+} [26]. The emission lines in cubic Gd_2O_3:Eu^{3+} corresponding to transition from $^5D_0 \rightarrow {}^7F_J$ ($J = 0$–4) manifolds of Eu^{3+}. The $^5D_0 \rightarrow {}^7F_J$ emission is a very sensitive for the crystal field around the Eu^{3+} sites. The Eu^{3+} $^5D_0 \rightarrow {}^7F_{1,3}$ is an allowed magnetic dipole transition, where as Eu^{3+}, $^5D_0 \rightarrow {}^7F_{2,4}$ is a forbidden electric dipole transition. However, this selection rule can be related when Eu^{3+} is placed in a host lattice lacking in inversion symmetry such as Gd_2O_3. It is well known that in a cubic Gd_2O_3 lattice has C_2 or C_{3i} (or S_6) sites for rare earth doping [27]. Because the rare earth ion occupying C_{3i} site possesses a centre of inversion symmetry, the $^5D_0 \rightarrow {}^7F_{2,4}$ optical transition is strictly forbidden. Therefore, the dominant $^5D_0 \rightarrow {}^7F_{1,3}$ rare earth emission lines originate from forced electric dipole transitions of the ion occupying C_2 sites (where there is a lack of inversion symmetry) and from allowed magnetic-dipole transitions. Specifically, the forced electric dipole transitions for Eu^{3+} ($^5D_0 \rightarrow {}^7F_{2,4}$) are hypersensitive to the host crystallographic symmetry [28]. Monoclinic Gd_2O_3: Eu^{3+} is known to have three nonequivalent C_s crystallographic sites for a rare earth ion doping [29]. Thus Eu^{3+} ions in different Gd_2O_3 crystal structures are expected to show different emission lines. The differences in the

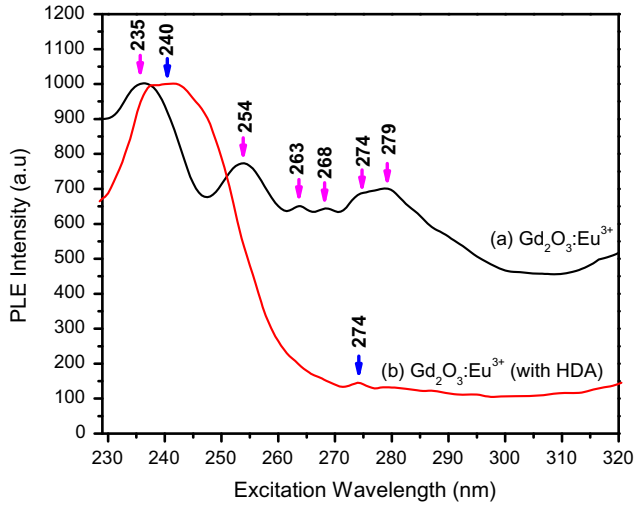

Fig. 11. PLE spectra of (a) Gd_2O_3:Eu^{3+} (without HDA) and (b) Gd_2O_3:Eu^{3+} (with HDA).

PL emission spectra of cubic versus monoclinic Gd_2O_3 lattice have been reported by various authors in thin films [30] and nanocrystallites [31]. The Eu^{3+} ion occupy Gd^{3+} site in the doped Gd_2O_3 samples,

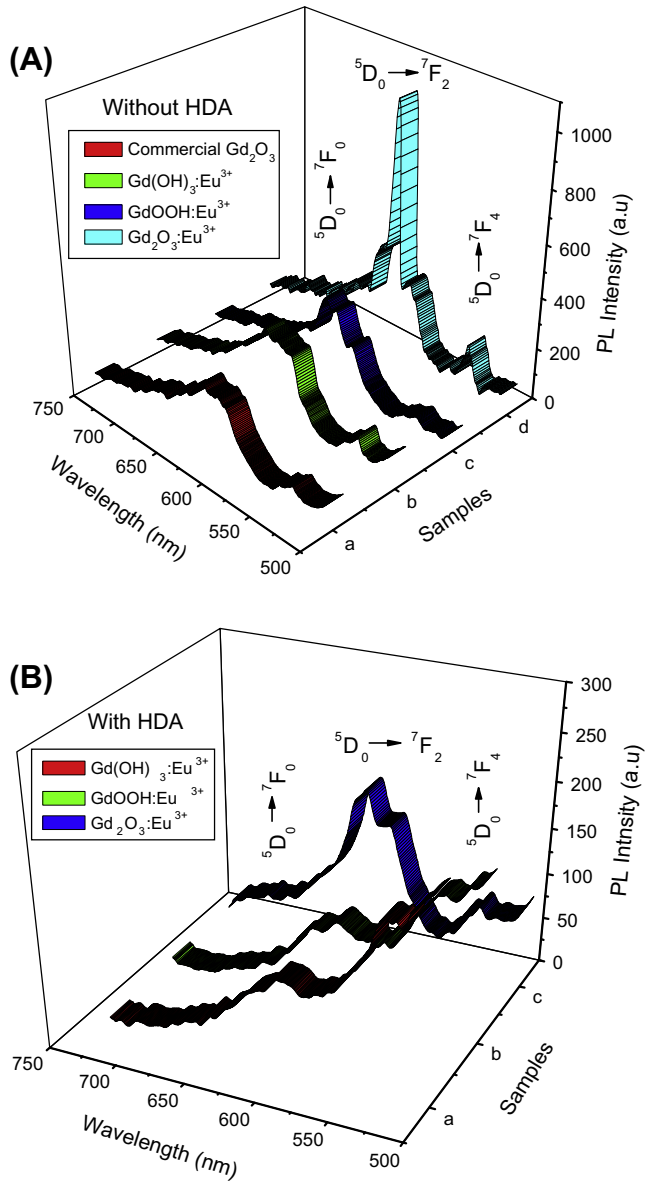

Fig. 12. (A) PL spectra of $Gd(OH)_3:Eu^{3+}$ prepared (without HDA) (a) as-prepared, (b) calcined at 350 °C and (c) calcined at 600 °C for 3 h. (B) With HDA) (a) as-prepared, (b) calcined at 350 °C and (c) calcined at 600 °C for 3 h.

resulting in the hypersensitive $^5D_0 \rightarrow {}^7F_2$ ($\Delta J = 2$) transition being the most prominent one in its emission spectrum. The intensity of the magnetic dipole transition ($^5D_0 \rightarrow {}^7F_1$) hardly changes with the crystal field strength around the Eu^{3+} ion, while the intensity of hypersensitive electric dipole allowed transition ($^5D_0 \rightarrow {}^7F_2$) is highly sensitive to structural changes and environmental effects in the vicinity of the Eu^{3+} ions.

It should be noted that the PL peaks of $Gd(OH)_3:Eu^{3+}$ nanorods are broaden as compared to those from cubic $Gd_2O_3:Eu^{3+}$. This broadening may result from the fact that a larger fraction of the Eu^{3+} ions will sit on the nanocrystals surface. The surface Eu^{3+} ions should possess a different disordered environment, which leads to inhomogeneous broadening of the emission peaks. The PL emission intensity is observed to be higher in $Gd_2O_3:Eu^{3+}$ when compared to other two phases. This is attributed to different crystal structures. Since, cubic Gd_2O_3 is known to be much more efficient host system for red emitting Eu^{3+} ion doping than the monoclinic counterpart. Another significant effect for low emission intensity is the surface states. Due to tiny dimensions of $Gd_2O_3:Eu^{3+}$ nanocrystals, it is possible

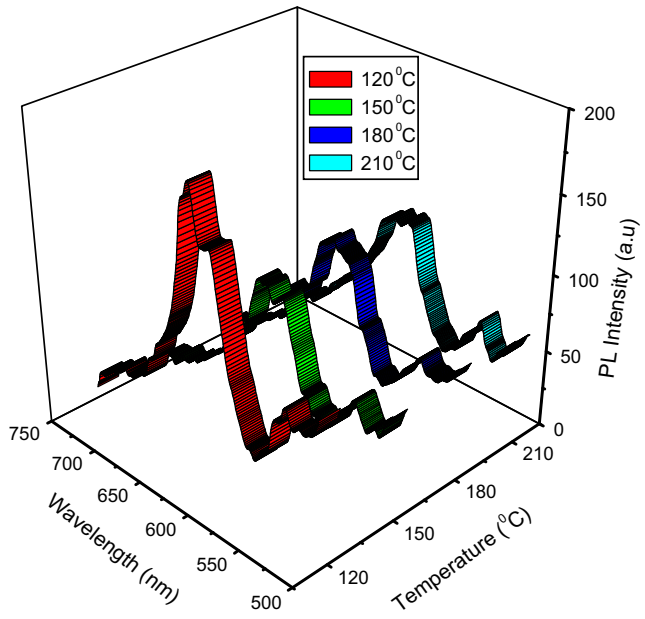

Fig. 13. PL of cubic $Gd_2O_3:Eu^{3+}$ (with HDA) at (a) 120 °C, (b) 150 °C, (c) 180 °C and (d) 210 °C for 24 h.

to speculate that surface states would play a considerable role in luminescence excitation energy which can be readily captured and quenched by surface states, leading to non-radiative relaxation.

4. Conclusions

Hexagonal $Gd(OH)_3:Eu^{3+}$, monoclinic $GdOOH:Eu^{3+}$ and cubic $Gd_2O_3:Eu^{3+}$ nanorods have been successfully synthesized by without and with HDA successfully by hydrothermal technique. FTIR studies reveal that HDA surfactant plays an important role in conversion of cubic to hexagonal phases. It is observed in presence of HDA surfactant, the particle is converted into rods of various sizes. TEM micrographs of $Gd(OH)_3:Eu^{3+}$ sample with HDA confirms smooth nanorods with various diameters in the range 20–100 nm. The effect of surfactant (HDA) on luminescence properties of various phases of Eu^{3+} doped $Gd(OH)_3$, GdOOH and Gd_2O_3 have been evaluated. It is observed that the optical band gap of $Gd(OH)_3:Eu^{3+}$ phase is more when compared to other two phases. These variations in optical band gap can be related to the degree of structural order–disorder into the lattice, which is able to change the intermediary energy level distribution within the band gap. The PL emission intensity is observed to be higher in $Gd_2O_3:Eu^{3+}$ when compared to other two phases. It should be noted that the PL peaks of $Gd(OH)_3:Eu^{3+}$ nanorods are broaden as compared to those from cubic $Gd_2O_3:Eu^{3+}$. This broadening may result from the fact that a larger fraction of the Eu^{3+} ions will sit on the nanocrystals surface. It is concluded that cubic Gd_2O_3 is known to be much more efficient host system for red emitting Eu^{3+} ion doping than the monoclinic counterpart. These studies reveal that Gd_2O_3 is a versatile material with high application potential in several technological fields (photonics).

Acknowledgments

One of the authors (H.N.) thanks to DST Nano Mission (Project No. SR/NM/NS-48/2010) New Delhi for sanction of the Project. One of the authors Prof. S.C. Sharma thanks to B.M.S. Educational trust and B.M.S. Institute of Technology for their continuous support.

References

[1] G.Y. Adachi, N. Imanaka, Chem. Rev. 98 (1998) 1479–1514.
[2] A.W. Xu, W.Y. Gao, H.Q. Liu, J. Catal. 207 (2002) 151–157.
[3] A.H. Peruski, L.H. Johnson, L.F. Peruski, J. Immunol. Methods 263 (2002) 35–41.
[4] N. Dhananjaya, H. Nagabhushana, B.M. Nagabhushana, B. Ruudraswamy, C. Shivakumara, R.P.S. Chakradhar, J. Alloys Comp. 509 (2011) 2368–2374.
[5] J. Dhanaraj, R. Jagannathan, T.R.N. Kutty, C.H. Lu, J. Phys. Chem. B 105 (2001) 11098–11105.
[6] N. Dhananjaya, H. Nagabhushana, B.M. Nagabhushana, R.P.S. Chakradhar, C. Shivakumara, B. Rudraswamy, Physica B 405 (2010) 3795–3799.
[7] B. Tang, J. Ge, C. Wu, L. Zhuo, J. Niu, Z. Chen, Z. Shi, Y. Dong, Nanotechnology 15 (2004) 1273–1276.
[8] G. Jia, K. Liu, Y.H. Zheng, K. Liu, Y.H. Song, H.P. You, H.J. Zhang, J. Phys. Chem. C 113 (2009) 6050–6055.
[9] C.R. Patra, R. Bhattacharya, S. Patra, N.E. Vlahakis, A. Gabashvili, Y. Koltypin, A. Gedanken, P. Mukherjee, D. Mukhopadhyay, Adv. Mater. 20 (2008) 753–756.
[10] N. Dhananjaya, H. Nagabhushana, B.M. Nagabhushana, B. Rudraswamy, C. Shivakumara, R.P.S. Chakradhar, Physica B 406 (2010) 1639–1644.
[11] N. Dhananjaya, H. Nagabhushana, B.M. Nagabhushana, B. Rudraswamy, C. Shivakumar, K.P. Ramesh, R.P.S. Chakradhar, Physica B 406 (2010) 1645–1652.
[12] K.H. Lee, Y.J. Bae, S.H. Byeon, Bull. Kor. Chem. Soc. 29 (2008) 2161–2168.
[13] X. Wang, Y. Li, Angew. Chem. Int. Ed. 41 (2002) 4790–4793.
[14] G. Liu, G. Hong, J. Wang, X. Dong, J. Alloys Comp. 432 (2007) 200–204.
[15] J. Zarembowitch, J. Gouteron, A.M. Lejus, J. Raman Spectrosc. 9 (1980) 263–265.
[16] D. Bloor, J.R. Dean, J. Phys. C 5 (1972) 1237–1252.
[17] Q. Mu, Y. Wang, J. Alloys Comp. 509 (2011) 2060–2065.
[18] N. Dilawar, S. Mehrotra, D. Varandani, B.V. Kumaraswamy, S.K. Haldar, A.K. Bandyopadhyay, Mater. Charact. 59 (2008) 462–467.
[19] C. Le Luyer, A. Garćıa-Murillo, E. Bernstein, J. Mugnier, J. Raman Spectrosc. 34 (2003) 234–239.
[20] L.K. Pan, Q. Sunchang, C.M. Li, J. Phys. Chem. B 108 (2004) 3404–3406.
[21] H.Q. Cao, X.Q. Qiu, B. Luo, Y. Liang, Y.H. Zhang, R.Q. Tan, M.J. Zhao, Q.M. Zhu, Adv. Func. Mater. 14 (2004) 243–246.
[22] J. Tauc, in: F. Abeles (Ed.), Optical Properties of Solids, North-Holland, Amsterdam, 1970.
[23] X. Liu, F. Zhou, M. Gu, S. Huang, B. Liu, C. Ni, Opt. Mater. 31 (2008) 126–130.
[24] G. Adachi, N. Imanaka, Chem. Rev. 98 (1998) 1479–1514.
[25] B. Liu, M. Gu, X. Liu, C. Ni, D. Wang, L. Xiao, R. Zhang, J. Alloys Comp. 440 (2007) 341–345.
[26] C. Louis, R. Bazzi, M.A. Flores, W. Zheng, K. Lebbou, O. Tillement, B. Mercier, C. Dujardin, P. Perriat, Solid State Chem. 173 (2003) 335–341.
[27] J. Yang, C.X. Li, Z.Y. Cheng, X.M. Zhang, Z.W. Quan, C.M. Zhang, J. Lin, J. Phys. Chem. C 111 (2007) 18148–18154.
[28] F. Vetrone, J.C. Boyer, J.A. Capobianco, A. Speghini, M. Bettinelli, Chem. Mater. 15 (2003) 2737–2743.
[29] M. Buijs, A. Meyerink, G. Blasse, J. Lumin. 37 (1987) 9–20.
[30] Geo. Rajan, K.G. Gopchandran, Appl. Surf. Sci. 255 (2009) 9112–9123.
[31] N. Dhananjaya, H. Nagabhushana, S.C. Sharma, B. Rudraswamy, N. Suriyamurthy, C. Shivakumara, R.P.S. Chakradhar, Appl. Phys. B 107 (2012) 503–511.